Environmental Pollution 361 (2024) 124810

Contents lists available at ScienceDirect

Environmental Pollution

journal homepage: www.elsevier.com/locate/envpol

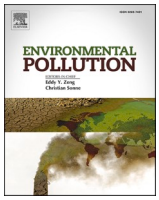

The relationship between the inhalation bioaccessibility of potentially toxic elements in road dust from a heavily polluted industrial area and the source of their pollution☆

Marija Zupančič [a], Miloš Miler [b], Gorazd Žibret [b,*]

[a] Faculty of Chemistry and Chemical Technology, University of Ljubljana, Večna pot 113, SI-1000, Ljubljana, Slovenia
[b] Geological Survey of Slovenia, Dimičeva ulica 14, 1000, Ljubljana, Slovenia

ARTICLE INFO

Keywords:
Coal mining
Inhalation bioaccessibility
Mining/smelting pollution
Potentially toxic elements
Road dust
Traffic pollution

ABSTRACT

One of the sources of chronic exposure to potentially toxic elements (PTE), especially in polluted environments, is the inhalation of resuspended road dust (RD). The aim of this study is to assess the inhalation bioaccessibility of PTE in RD from highly polluted environments from mining/smelting industries and traffic, and to identify any correlations between the bioaccessibility fraction of PTE and the physicochemical characteristics of the particles. RD from the studied area contains extremely high total concentrations of Cr, V, and Mn, which are likely due to pollution from the smelting industry. Additionally, elevated total concentrations of other elements associated with traffic emissions including Zn, Cu, Pb, Sb, and Sn were also measured. The bioaccessibility of PTE was assessed using two synthetic extraction solutions - Gamble's solution (GS) and Artificial Lysosomal Fluid (ALF). The majority of elements showed negligible bioaccessibility in GS. However, quite high inhalation bioaccessibility was observed for Zn, Pb, Sb, Cd, and Mn in the ALF solution, with a mean bioaccessible fraction of 49, 51.5, 41, 50, and 40% respectively. The highest bioavailable fraction was measured for Cd (97%) in a sample collected near a steel production facility and for Pb (95%) in a sample collected near the highway. These results indicate that increased mobility of the elements in inhaled particles occurs only in the case of phagocytosis. The lowest inhalation bioavailability was measured for Cr (mean is 3%). Differential individual particle analysis revealed that about 60% of phases, mostly major (Cr,Ti,V)-bearing metallic alloys, silicates, oxides and sulphides, are stable in ALF solution, while 40% of phases, mostly (Fe,Ca,Mn)-bearing oxides, silicates, sulphides, metals and metallic alloys originating from steel production, ferrochrome, ferrosilicon and vanadium production and from traffic emissions have been heavily corroded or completely dissolved. The study provides valuable information to further assess health hazards from various emission sources.

1. Introduction

Exposure to geogenic (mineral dust, windborne ash from wildfires, volcanic ash …), geoanthropogenic (dust generated from natural sources by human activities, e.g. farming) and anthropogenic dust particles (combustion and industrial processes, traffic) is associated with deterioration in human health and an increased risk of morbidity and mortality (Amato et al., 2013a,b). Particular attention must be paid to particles from the metal producing and processing industry, as they are the main carriers of potentially toxic elements (PTE) (Žibret and Rokavec, 2010; Žibret et al., 2013; Žibret, 2019; Potgieter-Vermaak et al., 2012; Corona-Sánchez et al., 2021). One of the major sources of atmospheric particulate matter in urban environment is resuspended road dust, sometimes also referred as street dust or street sediment (RD) (Fulvio Amato et al., 2013a,b; Chen et al., 2024; Weggeberg et al., 2019), which acts as a sink and a source of PTE. The RD consists primarily of soil derived minerals (up to 60%), mainly of quartz and to a lesser extent of clay forming minerals, organic matter (about 2%), that primarily originate from plants, while potentially toxic pollutants represent about 30% of the build-up (Gunawardana et al., 2012). During dry weather periods, the wind-related turbulence and the friction of tires of moving vehicles on dust-covered roads causes RD to become airborne (Jayarathne et al., 2019a). In addition to pollution from industrial sources, wear and tear of vehicle parts can also be an important source of RD pollution with PTE (Amato et al., 2009; Gunawardana et al., 2012;

☆ This paper has been recommended for acceptance by Hefa Cheng.

* Corresponding author.
E-mail address: Gorazd.Zibret@geo-zs.si (G. Žibret).

https://doi.org/10.1016/j.envpol.2024.124810
Received 19 June 2024; Received in revised form 7 August 2024; Accepted 22 August 2024
Available online 23 August 2024

Abbreviations

ALF	Artificial Lysosomal Fluid
DIPA	Differential Individual Particle Analysis
EDS	Energy Dispersive Spectroscopy
GS	Gamble's solution
LOD	Limit of Detection
OM	Organic Matter
PTE	Potentially Toxic Elements
RD	Road Dust
SEM	Scanning Electron Microscopy

Teran et al., 2020; Ali et al., 2017; Bardelli et al., 2011; Barrett et al., 2010; Dehghani et al., 2017; Liu et al., 2014; Shi et al., 2011; Stopford et al., 2003; Trojanowska and Swietlik, 2020; Świetlik et al., 2015). PTE-contaminated RD also poses a potential threat due to wash-off into the surrounding soil and stormwaters (Mahbub et al., 2010; Jayarathne et al., 2019b; Gunawardana et al., 2015). The build-up and wash-off of PTE from roads, carparks and other paved areas are highly influenced by traffic and rainfall characteristics (Mahbub et al., 2010; Gunawardana et al., 2012). The total dust build-up is a rapid process and can reach equilibrium within seven to nine days in a dry period (Egodawatta and Goonetilleke, 2008). RD undergoes constant physical and chemical transformations that strongly influence the size of the particles and the chemical species in which the PTE occur (Jayarathne et al., 2019a, 2018b). The processes of oxidation-reduction, surface precipitation, and adsorption change the chemical form of the original chemical species of PTE, which can drastically change their mobility and consequently their bioaccessibility (Jayarathne et al., 2017; Boim et al., 2021).

Exposure to PTE in environmental dust occurs primarily through ingestion (Gaberšek and Gosar, 2024), inhalation, and dermal contact (Corradi and Mutti, 2011; Jayarathne et al., 2018a). Due to the high cost, time and ethical concerns of in vivo animal toxicology studies, in vitro bioaccessibility studies are increasingly being used to assess potential human exposure to toxic elements (Cipullo et al., 2018; Witt et al., 2014). The bioaccessible amount of PTE is the fraction of the total PTE concentration that is soluble in body fluids and thus potentially available for uptake into the systemic circulation (Kastury et al., 2017). The most likely human exposure to PTE in RD is through inhalation. Numerous inhalation bioaccessibility extraction methods have been reported, but the lack of consensus on protocols often makes the data incomparable (Kastury et al., 2017; Zupančič et al., 2021; Drysdale et al., 2012; Guney et al., 2016; Guney et al., 2017; Hedberg et al., 2010; Kastury et al., 2020b; Kastury et al., 2020a; Wiseman et al., 2018; Monneron-Gyurits et al., 2024). In physiologically based in vitro extraction methods, extraction conditions are kept as close as possible to those of the respiratory system (Kastury et al., 2017; Colombo et al., 2008; Pelfrêne and Douay, 2018; Caboche et al., 2011). Only a few studies have emphasized the importance of characterizing solid phases containing PTE- and their behavior in simulated respiratory fluids (Hunt and Johnson, 2011; Miler, 2021). This is an important aspect that requires further detailed investigation.

Two simulated lung fluids which are the most commonly used as leaching agents are Gamble's solution (GS) and Artificial Lysosomal Fluid (ALF). GS, with a pH of 7.4, represents the neutral extracellular environment in the interstitium of the lung (Entwistle et al., 2019; Cánovas et al., 2023). The synthetic pulmonary ALF fluid, with a pH of 4.5 and a slightly higher organic matter content than in GS, simulates the lysosomal fluid of alveolar macrophages and is used to estimate the amount of soluble PTE phagocytosed during inflammatory processes in the human body (Colombo et al., 2008; Novo-Quiza et al., 2023).

RD has been used as a proxy for atmospheric contamination in many studies worldwide (Dietrich et al., 2022). Many of them speculate that long-term exposure to RD enriched with PTE poses a risk to human health (Chen et al., 2024 and references cited therein). The main purpose of our study was to investigate the relationship between the mobility of specific PTEs in road dust from an area with extremely high levels of PTE, particularly Cr and V, and the mineral composition of the samples and sources of pollution This study represents an upgrade of the study by Žibret et al. (2013) and investigated the bioaccessibility of 16 selected elements in detail. It includes 2 different simulations of digestion in body fluids, and the corresponding differential individual particle analysis (DIPA), which together provide an insight into the biochemical processes in the human body. A novel approach was used to assess sources of PTE based on characteristics and associations of solid PTE-bearing phases. The contribution of various solid PTE-bearing phases to the inhalation bioaccessibility of PTE was evaluated using in situ DIPA. This approach is essential for implementing appropriate remediation measures and effective control of pollution and its impacts on human health. RD samples collected from asphalt or concrete surfaces in the eMalahleni region (Republic of South Africa), where several sources of PTE pollution are combined, including coal mining, metal smelting industry and road traffic, were selected as a model system.

2. Materials and methods

The flowchart in Fig. 1 schematically presents the work done in this study and better illustrates its relation to previous work by Žibret et al. (2013).

2.1. Sample collection, preparation and analysis

Coal exploitation in the Witbank Coalfield began more than 125 years ago and still represents one of the most important coal mining areas in South Africa, providing the fuel for several South Africa's largest coal-fired power plants and is a supplier of energy to the extensive metallurgical industries (steel, ferrochrome, ferromanganese, vanadium and titanium) in the region (Hancox, 2016). RD sampling in 2011 identified numerous anthropogenic dust sources, including open-pit coal mines, metal smelters (Cr, V, Mn and others), coal-fired power plants and traffic. Extremely high levels of certain PTE were detected in the area, among the highest reported in the global scientific literature for RD (Žibret et al., 2013).

Detailed description of the sampling procedure can be found in the paper by Žibret et al. (2013). RD was collected on paved surfaces along roads or parking lots in areas of dust accumulation. Areas containing soil or plant debris were not sampled. Dust samples were collected in dry weather by plastic brushes and stored in PVC bags. Pre-analytical procedures included drying at 303 K and sieving under 0.125 mm mesh size. Sampling was conducted in the eMalahleni (formerly Witbank) surroundings in the Republic of South Africa (Fig. 2) in 2011. Approximately 200 g of the sample were collected in the field, while 5 g of pulps (<0.125 mm) were used for the determination of elemental content (Žibret et al., 2013), pH, organic matter and bioaccessibility (this study).

2.2. Analyses of RD samples

The thermogravimetric method, analogous to but extended from SIST EN 15169:2007 (Characterization of waste - Determination of loss on ignition in waste, sludge and sediments), was used to assess the organic matter (OM) content of RD samples (see details in the Supplementary Material). The pH of RD samples was determined according to SIST ISO 10390:2006 using a 1:5 (soil to liquid by volume) suspension in a 0.01 M $CaCl_2$ solution after 4 h of settling. Total PTE concentrations in RD samples were determined by ICP-MS at commercial laboratories (Bureau Veritas North America, Vancouver, Canada) after near-total digestion of the samples in a mixture of four acids ($HClO_3$, HNO_3, HCl and HF). Six analyses of geochemical standard material STD OREAS24P (internal standard of Bureau Veritas Laboratories) were used to verify

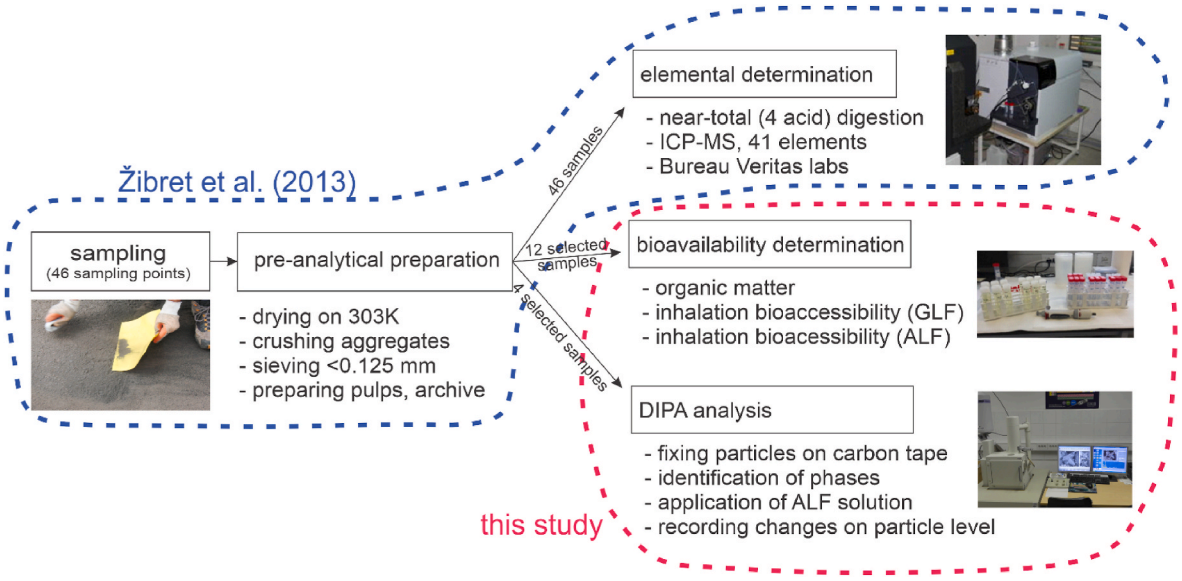

Fig. 1. The flow chart illustrating the work conducted in this study and its relation to the previous one.

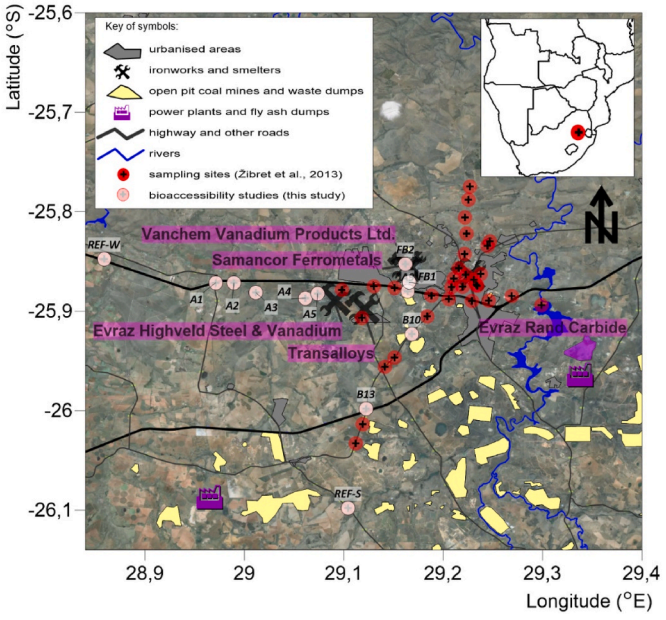

Fig. 2. The study area with the sampling sites and the locations of the main sources of PTE contamination.

accuracy. The quality of the laboratory results controlled with duplicates, repetitions, and blanks, was considered satisfactory. Detailed information, including additional quality control parameters, can be found in Žibret et al. (2013) and Žibret (2019). The limit of detection (LOD) of PTE values for bioaccessibility studies are summarized in Table S3.

2.3. Determination of the inhalation bioaccessibility of PTE

The definition of particle sizes used in inhalation exposure studies that simulate the inhalation pathway varies by research discipline and regulatory agencies (Colombo et al., 2008; Kastury et al., 2017). Although by definition only particles with a diameter of less than 100 μm can potentially be deposited in the respiratory system, when the amount of inhaled air is increased, e.g., during heavy work or intense exercise, particles with larger dimensions can also be deposited in the tracheobronchial parts of the airway. Due to hygroscopicity, soluble chemical species can dissolve from inhaled particles, changing the size of the particles and influencing their deposition, clearance and retention (Kastury et al., 2017). In addition to the composition of the extraction solution, the amount of PTE extracted from RD samples during extraction tests to determine bioaccessibility depends strongly on the solid/-liquid ratio and the extraction time (Caboche et al., 2011). Table S1 summarises the experimental conditions used in published studies to determine the inhalation bioaccessibility of PTE in particulate media.

The inhalation bioaccessibility of PTE in selected RD samples (N = 12; <0.125 mm) from the eMalahleni industrial area was evaluated using two synthetic lung solutions: Gamble's solution (GS) and Artificial Lysosomal Fluid (ALF). The first simulates the extracellular environment in the interstitium, while the ALF mimics the lysosomal fluid of alveolar macrophages. Although several compositions of these two simulated fluids have been reported, the composition of the solutions according to Colombo et al. was adopted in our study (Colombo et al., 2008; Expósito et al., 2021).

The results of previous studies have shown that metal release rates in pulmonary surfactants decrease with increasing particle loading (Caboche et al., 2011), especially at high loadings (S/L < 1/50).This led us to decide to conduct inhalation bioaccessibility in this study with an S/L ratio of 1/100. Although some studies have shown that dissolution of PTE occurs rapidly within the first few hours of extraction and then asymptotically approaches equilibrium (Caboche et al., 2011), the amount and residence time of inhaled particles strongly depend on differences in intensity of respiration and health conditions, which can significantly prolong their retention time. Therefore, an extraction time of 168 h (1 week) was selected for this study.

The concentration of Fe in GS and ALF solution extracts, obtained after conducting the inhalation bioaccessibility test performance was determined by AAS (Varian AA 240), while the concentrations of Cr, Mn, V, Ni, Co, Cu, Zn, Pb, Sb, Sn and Cd were determined by ICP-MS (Agilent 7500ce). An extraction run consisted of the test samples (in triplicate) and extraction blanks (in sixth replicate). Due to the high salt content in the synthetic liquids, the samples and blank solutions analysed by ICP-MS were diluted 50-fold. The calibration standard solutions were prepared using the same solution matrix as the prepared samples and blanks. The limit of detection (LOD) for specific elements was calculated as a concentration equal to three times the standard deviation of the mean element concentration in the blank samples (N = 6) and is shown

in Table S4.

The results of total and bioaccessible PTE concentrations were processed using descriptive statistics and Spearman's rank correlation coefficients. Additionally, analysis of variance (One-way ANOVA, $\alpha = 0.05$) was conducted to assess statically significant differences in the PTE bioaccessibility data.

2.4. Scanning electron microscopy/energy dispersive spectroscopy (SEM/EDS) and differential individual particle analysis (DIPA)

The identification of solid mineral and amorphous PTE-bearing phases in selected RD samples (A3, A5, B10, FB2) and qualitative assessment of their potential sources were performed using SEM/EDS. The assessment of their contribution to inhalation bioaccessibility was carried out by in situ DIPA according to Hunt & Johnson (2011). Samples were prepared using two methods: (1) polished sections were prepared by embedding dust material in epoxy resin, followed by grinding with carborundum and fine polishing using 6 μm, 3 μm and 1 μm diamond suspension fluids and (2) rough samples were prepared by mounting particles on a double-sided carbon tape and removing excess particles with compressed air. All samples were coated with a thin layer of carbon for conductivity. Prior to reaction, solid PTE-bearing phases were identified and characterised by their shape, size and semi-quantitative chemical composition by using JEOL JSM 6490LV SEM coupled with Oxford INCA Energy 350 EDS system in the back-scattered electron (BSE) mode at accelerating voltages of 10–20 kV, spot size of 28–48, working distance of 10 mm and spectrum acquisition time of 60 s. Afterwards, ALF solution was applied by a pipette and kept wetted with ALF in dark at 37°C for 168 h, while the solution was exchanged daily. After the elapsed reaction time, reagent was removed with a pipette and neutralized with Milli-Q water. After digestion, the same phases (particles) were observed again by SEM/EDS to record changes, including particle size, shape, and composition. Potential mineral equivalents of solid phases were assessed from the atomic proportions of the constituent elements, acquired by EDS point analysis, and compared with the atomic proportions of constituent elements in known stoichiometric minerals from mineral databases (Anthony et al., 2009; Barthelmy, 2012). The software was calibrated for quantification using premeasured universal standards included in the EDS software, according to fitted standards procedure, referenced to a Co optimisation standard (Goldstein et al., 2003). The correction of EDS data was performed on the basis of the standard ZAF-correction procedure included in the INCA Energy software (INCA, 2006).

3. Results

3.1. Total metal concentrations, organic matter content and pH of RD samples

The results of elemental analyses of the RD from eMalahleni ($N = 12$) and the descriptive statistics of the data are summarized in the supplementary material (Table S3). The RD samples are highly enriched with Fe, Cr, Mn, Ni and V. The levels of Cu, Zn, Pb, Sb, Sn and Cd are comparable to or lower than the concentrations found in RD from other industrially polluted locations around the world (Zhang and Wang, 2009; Duong and Lee, 2009; Potgieter-Vermaak et al., 2012). According to Žibret et al. (2013) samples A4 and A5 were heavily impacted by steel and vanadium industry, while samples FB1 and FB2 by the ferrochrome industry.

The lowest pH was observed in sample A2, which represents a slightly metal contaminated sample and also contains the lowest Cr concentrations of all samples, while the highest pH values were found in samples A4 and A5, which were heavily contaminated with PTE (mainly Fe, Mn and V). A very high variability between the samples can be observed in the organic matter (OM) content, with the highest value found in sample B13, which was less contaminated with PTE. Both parameters, the pH and the OM content, can have a considerable influence on the retention (build-up) of PTE in RD and their bioaccessibility.

3.2. Bioaccessibility of PTE in synthetic lung fluids

The results of the inhalation bioaccessibility of PTE in RD showed that the PTE solubility in GS is very low. The concentrations of Fe, Co, Zn, Pb, Sb, Sn and Cd are even lower than the LOD for all RD samples (Table S4). The pH of the GS extracts ranged from 7.99 to 8.38 (sample A5). A strong correlation with the pH of solid samples was observed ($r_s > 0.77$).

Significantly higher solubility of PTE was observed in ALF solution with pH of extracts ranging from 4.63 to 4.77. The descriptive statistics of PTE concentrations in GS (for the results above the LOD) and ALF solutions are presented in Fig. 3. The highest values of individual PTE concentrations from ALF solutions were measured for Fe, followed by Zn, V and Cr.

The bioaccessible fractions of total PTE in individual RD samples are presented in the supplementary material (Figs. S1 and S2, and Table S5). The results show that the highest percentage of the PTE bioaccessible fraction in GS solution is accounted for V, followed by Ni, Mn, and Cu,

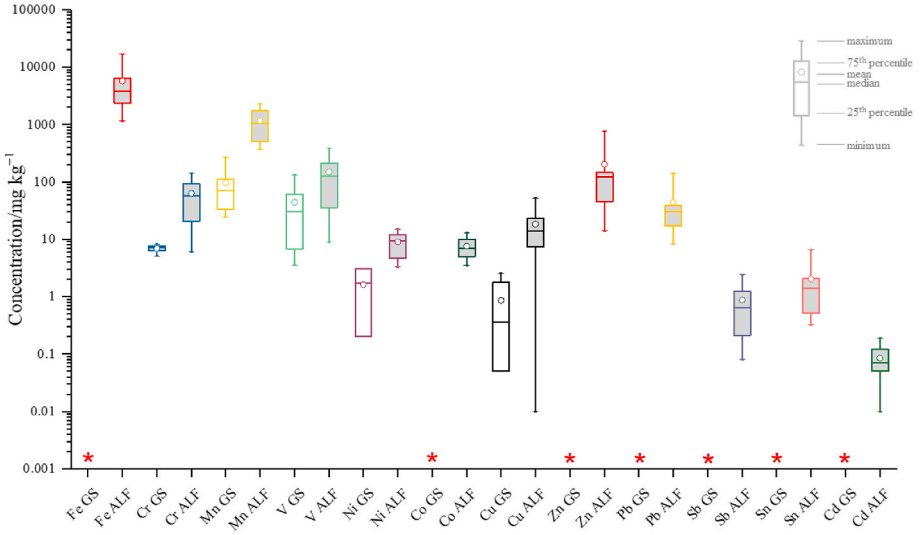

Fig. 3. Descriptive statistics of PTE concentrations in GS (white boxes) and ALF (gray boxes) extracts. * indicated that most of the measurements were below detection limit.

while Cr is generally not bioaccessible. The observed bioaccessible fractions of PTE in ALF solution are much higher, the highest (>40%) were measured for Zn, Pb, and Sb, while the lowest (<20%) for V, Ni, Fe, and Cr.

3.3. SEM/EDS (DIPA)

In this subchapter, the results of the Differential Individual Particle Analysis (DIPA) of 4 selected RD samples with the highest total PTE concentrations are presented.

3.3.1. Identification of the solid PTE-bearing phases and assessment of their source

A total of 111 particles were analysed in four selected samples and apportioned to 53 different types or phases. These phases are major solid carriers of Fe, Cr, Mn, V, Ni, Zn, and Pb as well as Cu and Co. Identified phases, together with their grain sizes and abundances are presented in Table S6, while their elemental composition is shown in Table 1.

In all investigated samples, 40 phases were intergrown with each other and were grouped into 8 groups (Table 2). No distinctive associations were found in 13 phases, which were classified as ungrouped. Particulate materials collected directly from individual sources, which could be used to directly link emission source with a specific phase group in RD, were not available for this study. However, the sources of these phases were indirectly assessed based on i) spatial distribution of elements in RD (Žibret et al., 2013), ii) typical elemental and mineralogical characteristics of each of 8 phase groups, iii) the number of phases in the samples and the combinations of constituent elements in them and by iv) considering literature data on the mineral and elemental composition of raw materials, slags and products used and produced at

Table 1
Mean elemental composition (wt%) of the phases identified in selected RD samples determined by EDS analysis.

Phase	n	Elemental composition (wt.%)																
		O	Na	Mg	Al	Si	P	S	K	Ca	Ti	V	Cr	Mn	Fe	Ni	Zn	Pb
Fe-O	1	40.5				0.7		0.3							58.8			
Fe-O(Al,Si)	1	40.4			3.3	3.1				1.2					52.1			
spher. Fe-O(Mn)	2	30.7												0.9	68.4			
spher. Fe-O(Ti)	1	33.6		0.9		0.4				1.4	0.4				63.3			
Fe-O(V,Cr)	1	42.1		0.7		0.3		0.3		1.3		1.6	0.5		53.3			
Fe-O-Ti(V,Mn,Cr)	5	34.3		0.6	1.4						8.9	0.8	0.3	0.3	53.4			
Fe-Ti-O(Mn)	3	36.4		1.0							28.6			3.3	32.4			
Ti-O	3	44.5			0.2	0.2				0.1	54.5				0.5			
Ca-Ti-O	3	42.3			0.3					26.0	31.3				0.1			
Mg-Al-O(Ti)	4	43.2		15.9	29.5					0.1	4.2	3.5	1.6	0.3	1.6			
Ti-Mg-Al-O(V,Mn)	4	42.3		7.2	1.8					0.3	46.1	1.3		0.2	0.8			
Mg-Al-Cr-O	4	43.6		13.9	21.0						0.2		19.6		1.6			
Cr-Mg-Al-O(V,Mn,Fe)	1	35.1		11.4	1.4					0.9		1.5	48.4	0.7	0.6			
Fe-Cr-Mg-Al-O	11	37.2		7.8	7.8						0.4	0.1	31.4		15.3			
Fe-Cr-Al-Zn-Mg-O	1	43.1		1.5	9.7	0.3					0.3		18.7	2.1	19.5		4.7	
Ca-Fe-Al-V-O(Cr)	1	33.5		0.5	7.5	0.5				31.8	1.0	4.3	1.3		19.6			
Ca-Fe-V-O(Ti,Si,Al)	2	34.9			2.1	0.8				28.4	0.5	2.6		0.3	30.6			
Mg-Fe-O(Mn,Cr)	1	36.2		38.9						0.5			0.7	1.2	22.6			
Fe-Mn-Mg-O(Cr)	1	28.7		5.5						0.8			0.7	10.3	53.9			
Fe-Mg-Mn-Ca-O(Cr)	1	29.9		5.3						4.7			0.6	7.9	51.5			
Fe-Mg-Mn-Cr-O	1	31.4		20.8						0.9			1.3	4.7	40.9			
Fe-V-Ti-Mn-Cr-Al-O	1	23.4			1.4						7.0	26.8	4.7	7.4	29.4			
V-Fe-Cr-Mg-Al-Ti-Mn-O	1	27.1		4.0	3.1					0.2	3.9	26.2	9.2	2.4	24.0			
Ca-Si-O	1	48.6	0.5	0.6	0.3	21.5	1.3	1.6		22.2		0.6		0.6	2.2			
Mn-Si-O	1	39.7				21.4				0.2				38.7				
Mg-Al-Si-O	2	49.9	0.5	11.5	8.3	23.8		0.3	0.3	2.1	0.7		1.9		1.0			
Si-Al-Ca-Fe-K-Na-O	1	49.8	0.9		7.1	25.7			2.1	4.7	0.8	0.7		2.5	5.7			
Si-Ca-Mg-Al-Ti-O(Mn)	5	47.1		7.2	6.2	16.3				14.5	7.2	0.1		0.5	0.9			
Si-Ca-Mg-Fe-Al-O(Ti,Mn,V)	1	46.5	0.6	5.3	3.4	19.6				13.1	1.9	0.5		1.0	8.0			
Si-Ca-Mn-Mg-O	1	44.0		2.6		23.1				14.6				15.7				
Si-Fe-Ca-Mg-Mn-Al-O(V,Ti)	1	41.0		4.8	0.3	15.5				12.6	0.3	0.4		3.9	21.3			
Si-Ca-Mg-Al-O(Cr,Ti)	1	48.4		7.5	6.8	20.5				14.8	0.9		1.2					
Ca-Si-Mn-Mg-Al-O	2	44.1	0.2	2.4	1.8	22.3		0.5	0.5	17.9				10.5				
spher. Mg-Si-Ca-Al-O(S,Cr)	1	48.8		23.9	3.0	15.6				4.3			3.7		0.8			
Mg-Si-O(Cr)	1	47.9		30.4	0.3	19.2				0.9			0.6		0.8			
spher. Fe-Al-Si-O(V,Ti)	1	37.5			19.5	3.6					0.6	0.8			37.9			
spher. Fe-Si-Al-O(V,Ti,S)	1	36.3			4.0	12.0		0.5		0.5	0.3	0.3		0.5	45.6			
$Fe-S_2$	2							55.8							44.2			
Mn-S	1	7.5				2.9		32.9		1.6				54.3	0.8			
(Fe,V,Cr)-S	1							40.7				14.6	3.0		41.7			
Cr-Fe-S	1							47.6			0.35		43.57	0.87	7.6			
Mn-Si-Fe	5					24.4					0.1			61.0	14.5			
Mn-Fe-Si	6					12.6	0.2			0.1				72.5	14.6			
Fe-Si-Cr	1					15.6							6.9		77.5			
Fe-Cr-Si	1					12.0						0.4	35.7		51.8			
Cr-Fe-Si	1	2.6				0.5						0.6	72.3		24.0			
V-Ti(Cr)	1										17.0	79.1	1.8		2.2			
Ti-Cr-V	1				0.4						74.8	3.6	20.1		1.2			
Fe(Cr,Ni)	2												3.9		95.3	0.8		
Fe(Cr,V)	2	4.3		1.3	1.0							1.7	4.7	0.2	86.8			
Fe-Cr	1	1.8						0.4					35.8		62.1			
Cr_3-Fe(V)	5	0.5										0.5	73.0	0.2	25.8			
Pb	1					14.2								41.5	10.7			33.6

n – number of analyses.

Table 2
Phase groups determined according to phase associations in selected RD samples and their potential sources.

Group 1	Group 2	Group 3	Group 4	Group 5
A5	B10	A3, A5	A3	A5
EHS	SC/VC	EHS, RT	EHS	EHS
Mg-Al-O(Ti) Si-Ca-Mg-Al-Ti-O(Mn) Ti-Mg-Al-O(V,Mn) Ca-Ti-O	Ca-Fe-Al-V-O(Cr) Ca-Si-O Mg-Fe-O(Mn,Cr)	Ca-Fe-V-O(Ti,Si,Al) Fe-Mg-Mn-Ca-O(Cr) Fe-O(Al,Si)	Fe-V-Ti-Mn-Cr-Al-O Si-Al-Ca-Fe-K-Na-O	Si-Ca-Mg-Fe-Al-O(Ti,Mn,V) Si-Fe-Ca-Mg-Mn-Al-O(V,Ti) V-Fe-Cr-Mg-Al-Ti-Mn-O
Group 6	**Group 7**	**Group 8**	**Ungrouped**	**Potential sources**
FB2	**A3, A5, B10, FB2**	**A5, B10, FB2**	**phases**	**for ungrouped**
SC/VC	**SC/VC, EHS, RT**	**EHS, SC/VC**		**phases**
Mn-S Si-Ca-Mn-Mg-O	(Fe,V,Cr)-S Cr-Fe-Si Cr-Mg-Al-O(V,Mn,Fe) Fe(Cr,Ni) Fe(Cr,V) Fe-Cr Fe-Cr-Mg-Al-O Fe-O Fe-O(V,Cr) Mg-Al-Cr-O Mg-Al-Si-O Mg-Si-O(Cr) Si-Ca-Mg-Al-O(Cr,Ti) spher. Fe-Al-Si-O(V,Ti) spher. Fe-Si-Al-O(V,Ti,S) spher. Mg-Si-Ca-Al-O(S,Cr) Ti-Cr-V V-Ti(Cr)	Ca-Si-Mn-Mg-Al-O Mn-Fe-Si Mn-Si-Fe Mn-Si-O Pb	spher. Fe-O(Mn) spher. Fe-O(Ti) Fe-O-Ti(V,Mn,Cr) Fe-Ti-O(Mn) Fe-Cr-Al-Zn-Mg-O Fe-Mn-Mg-O(Cr) Fe-Mg-Mn-Cr-O Fe-S_2 Cr-Fe-S Fe-Si-Cr Fe-Cr-Si Cr_3-Fe(V) Ti-O	EHS EHS EHS, G EHS, G SC/VC, RT EHS EHS LC/AA, RT SC/VC SC/VC SC/VC SC/VC EHS, RT, G

EHS – Evraz Highveld Steel
SC/VC – Samancor Chrome, Vanchem
LC/AA – Landau Colliery/Anglo-American
RT – Road Traffic
G – Geological bedrock

different possible local anthropogenic sources (Nkohla, 2006; Diao et al., 2009; Steinberg et al., 2011; Mokwena, 2012; Perimal, 2013; Ringdalen et al., 2013; JMA Consulting, 2014; Samancor Chrome, 2018; Horckmans et al., 2019; Gao et al., 2021; Yang et al., 2023). as well as the geological bedrock of the study area (Africa GeoPortal, 2023) and solid PTE-bearing species typical of traffic emissions (e.g. Miler, 2021 and references therein). All phases containing PTE, associated with a phase group typical for a specific source in terms of chemistry, mineralogy and morphology, were assumed to share the same origin. The assessment of sources indicate that more than half of the phases (groups 1, 4, 5, partly also groups 3, 7, 8) originate from metallurgical processes in the nearby steel production. One third of the phase groups originated from ferrochrome, ferrosilicon and vanadium production (groups 2, 6, partly also groups 7, 8) with a minimal contribution from road traffic (some phases in groups 3, 7, some ungrouped phases), geological bedrock, coal mining (Landau Colliery/Anglo-American) and coal-firing power plants (some ungrouped phases) (Table 2).

3.3.2. Assessment of the contribution of solid PTE-bearing phases to bioaccessibility of PTE

The DIPA exposed to ALF solution showed very different phase reactions. Most phases (60%) remained unaffected, including stable silicate, oxide, and sulphide minerals, as well as metallic alloys originating predominantly from steel production. These phases mostly contain Cr, Ti, and V as major constituent elements (Table 3).

Around 40% of the phases experienced significant changes in their physico-chemical properties during the reaction (Fig. 4). Unstable phases consist of unstable oxide, silicate, and sulphide minerals, as well as metals and metallic alloys that mostly originate from steel production, ferrochrome, ferrosilicon, vanadium production, and road traffic emissions. These phases contain Fe, Ca and Mn as major constituent elements (Table 3). Completely dissolved oxide phases are Fe-oxides with V and Cr (Fig. 4a), Ca-Fe-(Al)-V-oxides with Cr and Ti (Fig. 4b), Mg-Fe-oxides with Mn and Cr, and Fe-Mg-Mn-Cr-oxides. The dissolved silicate phases include Ca-silicates, Ca-Mn-Mg-Al-silicates (Fig. 4c), Fe-Ca-Mg-Mn-Al-silicates with V and Ti, Mg-silicates with Cr and spherical Fe-Al-silicate with V, Ti, and S, as well as spherical Mg-Ca-Al-silicates with Cr and S. Mn sulphides Mn-Fe-Si (Fig. 4d), metallic Fe with Cr, Ni and V (Fig. 4e), and metallic Pb (Fig. 4f) were also found to be unstable under ALF solution. Larger grains of metallic Fe with minor Cr and V (Fig. 4a) were also significantly corroded, partially oxidised and, in addition, the V content decreased by 0.7 wt%, which was ascribed to leaching. Some dissolved phases were replaced by secondary phases. Dissolved Fe-Mg-Mn-Cr-oxides were replaced by precipitates of Cr-Fe-Ca-Na-Cl-Si-oxides, while Ca-silicates, Ca-Mn-Mg-Al-silicates and Mn-Fe-Si alloys were replaced by Si-oxides (quartz) (Fig. 4c and d). Partially or selectively dissolved phases include spherical Fe-oxides with Mn, and Ca-Mn-Mg-silicates. Spherical Fe-oxides with Mn showed partial selective dissolution of parts with higher Fe and Mn content, resulting in a somewhat lowered surface. Ca-Mn-Mg-silicates had significantly corroded surfaces, particularly along fractures. Phases that showed no visible changes, but partly changed their composition, are Cr-Fe-sulphides and Fe-Cr alloys (ferrochrome). The Cr-Fe-sulphides were partly oxidised, while in Fe-Cr alloys the content of Cr decreased by 8 wt%.

Table 3
Changes in the phases identified in selected RD samples after exposure to ALF solution.

Phase	Sample			
	A3	A5	B10	FB2
Fe-O		NC		
Fe-O(Al,Si)	NC			
spher. Fe-O(Mn)	PD, SD	PD, SD		
spher. Fe-O(Ti)	NC			
Fe-O(V,Cr)		CD		
Fe-O-Ti(V,Mn,Cr)	NC	NC	NC	NC
Fe-Ti-O(Mn)	NC	NC	NC	
Ti-O		NC	NC	
Ca-Ti-O		NC	NC	
Mg-Al-O(Ti)		NC		
Ti-Mg-Al-O(V,Mn)		NC		
Mg-Al-Cr-O			NC	NC
Cr-Mg-Al-O(V,Mn,Fe)				NC
Fe-Cr-Mg-Al-O	NC	NC	NC	NC
Fe-Cr-Al-Zn-Mg-O		NC		
Ca-Fe-Al-V-O(Cr)			CD	
Ca-Fe-V-O(Ti,Si,Al)	CD			
Mg-Fe-O(Mn,Cr)			CD	
Fe-Mn-Mg-O(Cr)	NC			
Fe-Mg-Mn-Ca-O(Cr)	NC			
Fe-Mg-Mn-Cr-O	CD, R (Cr-Fe-Ca-Na-Cl-Si-O)			
Fe-V-Ti-Mn-Cr-Al-O	NC			
V-Fe-Cr-Mg-Al-Ti-Mn-O		NC		
Ca-Si-O			CD, R (Si-O)	
Mn-Si-O		NC		
Mg-Al-Si-O			NC	
Si-Al-Ca-Fe-K-Na-O	NC			
Si-Ca-Mg-Al-Ti-O(Mn)		NC		
Si-Ca-Mg-Fe-Al-O(Ti,Mn,V)		NC		
Si-Ca-Mn-Mg-O				PD, CS
Si-Fe-Ca-Mg-Mn-Al-O(V,Ti)		CD		
Si-Ca-Mg-Al-O(Cr,Ti)				NC
Ca-Si-Mn-Mg-Al-O		PD, CS	CD, R (Si-O)	
spher. Mg-Si-Ca-Al-O(S,Cr)	CD			
Mg-Si-O(Cr)	CD			PD
spher. Fe-Al-Si-O(V,Ti)		NC		
spher. Fe-Si-Al-O(V,Ti,S)		CD		
$Fe\text{-}S_2$			NC	NC
Mn-S				CD
(Fe,V,Cr)-S		NC		
Cr-Fe-S				NC, PO
Mn-Si-Fe		NC		NC
Mn-Fe-Si		CD, R (Si-O)	CD	
Fe-Si-Cr				NC
Fe-Cr-Si				NC
Cr-Fe-Si				NC
V-Ti(Cr)		NC		
Ti-Cr-V				NC
Fe(Cr,Ni)			CD	CD
Fe(Cr,V)		CS, PO, CC (V, Fe)		CD
Fe-Cr	NC, CC (Cr)			
$Cr_3\text{-}Fe(V)$		NC	NC	NC
Pb				CD

NC - no visible changes.
PD - partly dissolved.
SD - selectively dissolved.
CD - completely dissolved.
PO - partly oxidized.
CS - partly oxidized.
R - replaced.
CC - changes in element content.

Additional phases, carriers of Mn, Cr, Zn, Cu, Ni, and Co, were identified in rough particle samples from sampling sites A3, B10, and FB2. In sample A3, the identified phases include Mn-Al-silicates with Zn, Fe-Al-Zn-silicates, Ca-Al-Mn-oxides with Ni, and Fe-Cu-sulphides (chalcopyrite). Apart from Fe-Cu-sulphides, all other phases were partially dissolved, resulting in 6–13% reduction in their size. Fe-Cu-sulphides showed no visible dissolution, but precipitates of Cu-sulphide (covellite) formed on its surface, indicating leaching of Cu. In sample FB2, Fe-Cr-oxides with Zn and Fe-Cr-Si alloy with Ni were unaffected during the reaction. In contrast, in sample B10, a small inclusion of (Mn,Ba)-oxide with Co, within a grain of Fe-oxide with minor Si and Al was completely dissolved after the reaction.

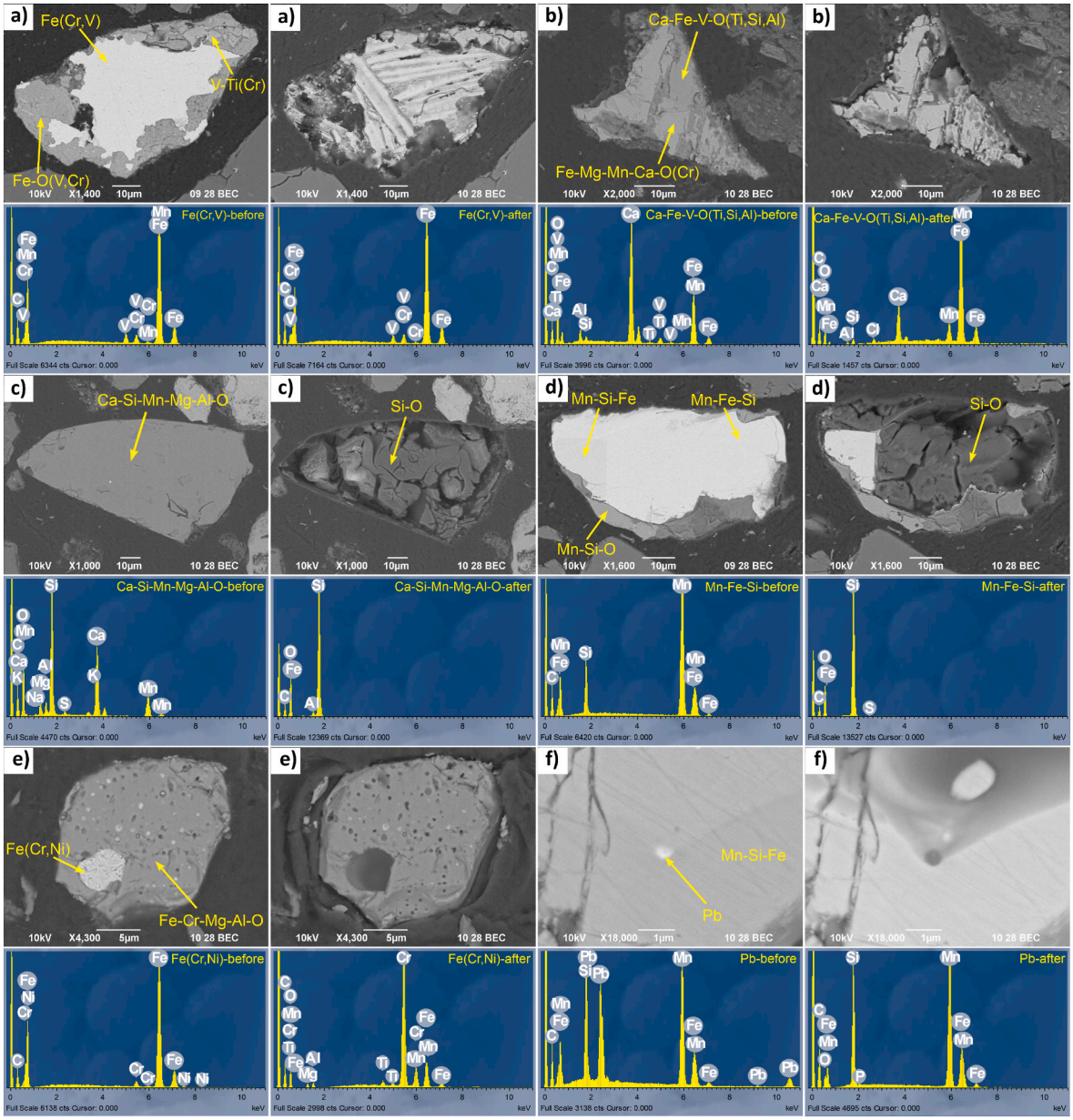

Fig. 4. SEM (BSE) images and EDS spectra of representative PTE-bearing phases before and after exposure to the ALF solution.

4. Discussion

4.1. Inhalation bioaccessibility of elements associated with the metal smelting industry

The pollution of RD from eMalahleni with PTE is mainly associated with two important sources - the metal smelting industry and road traffic. Coal mining and metal smelting industries are the main sources of high concentrations of Fe, Cr, Mn, V, Ni, and Co in RD (Žibret et al., 2013). While concentrations of Fe and Co in the GS extracts are below the LOD (<10 mg kg^{-1} and <0.2 mg kg^{-1}, respectively) the bioaccessibility of the other four elements increases in the range Cr < Mn < V < Ni (Fig. S1, Table S4).

The total Fe concentrations in the RD samples used in this study are very high, ranging from 3.8% to 11.7% of the total sample mass (Table S3). While the Fe concentrations in the GS extracts are below the LOD, the solubility of Fe in ALF reaches up to 1.7% of the total sample mass. The negligible mobility of Fe species in GS has also been perceived by Hedberg et al. (2010) and Guney et al. (2017). The bioaccessibility of Fe in RD samples (Fig. S1) ranges from 1.6% to 26.1% of the total Fe content and shows a high correlation with the bioaccessibility of Cr and Ni. The sample A3 has the highest Fe bioaccessibility, indicating that the pollution is associated with PTE characteristic of road traffic. Hedberg et al. (2010) investigated the bioaccessibility of Fe and Cr in various commercially relevant forms and alloys. They discovered that the bioaccessibility of Fe was significantly higher in pure Fe particles, followed by stainless steel, and much lower in alloys. The results are consistent with the potential sources of contamination of our samples as well as their bioaccessibility. The results of DIPA show that the contribution of phases to the bioaccessibility of Fe follows this order: metallic Fe with minor Cr and V > Mn-Fe-Si alloys > spherical Fe-Al-silicates with V, Ti and S > Fe-Mg-Mn-Cr-oxides > metallic Fe with Cr and Ni > Fe-oxides with V and Cr > Ca-Fe-V-oxide with Ti.

The most Cr-contaminated RD sample is FB2, followed by samples A9 and FB1. All of them are located in the vicinity of Cr production facilities. The total Cr concentrations in other RD samples are lower, although still high compared to RD globally. The bioaccessibility of Cr in the GS solution is low and ranges from 0.02% to 1.61% (Table S5). The

solubility of Cr in ALF is lower than the solubility of Fe, with a bioaccessibility of 0.16%–14.0%, which also corresponds to the study of Hedberg et al. (2010). The highest bioaccessibility of Cr found in samples from this study, in both GS and ALF, is comparable to the bioaccessibility of Cr reported for RD from busy inner city roads (Potgieter-Vermaak et al., 2012; Pelfrêne et al., 2017). The lowest bioaccessibility of Cr (<0.5%) is observed in samples that are associated with pollution from Cr production. The results are in line with the DIPA analyses, showing that metallic Fe with Cr and V contributes the most to Cr bioaccessibility, followed by spherical Mg-Ca-Al-silicates with Cr and S, metallic Fe with Cr and Ni, and the lowest contribution is from Fe-Mg-Mn-Cr-oxides. Contrary, all phases with high Cr content, which are most probably the result of emissions from the Cr smelting industry, show no visible changes after exposure to the ALF solution.

Mn ($r_s = 0.61$) and V ($r_s = 0.54$) are the only elements that show a statistically significant correlation with the organic matter content in the RD samples in this study. The mobility of Mn in GS solution is much higher than that of Fe and Cr and ranges from 0.52% to 6.43%. The samples from heavily contaminated areas are showing the lowest bioaccessibility. The highest measured bioaccessibility of Mn in ALF is 59%, which is much higher than the corresponding value for Cr (14%). Although the mobility of Mn is lower in most Mn contaminated samples compared to non-contaminated ones, it is still above 30%. The DIPA results showed that complete dissolution was observed for Mn containing phases of Mn-Fe-Si alloys, Ca-Mn-Mg-Al-silicates, and Mn sulphides.

The total concentration of V showed a strong correlation with the distance of the sample site from the Evraz Highveld Steel plant (Žibret et al., 2013). The bioaccessibility of V in GS is the highest of all six elements associated with the emissions from the metal smelting industry (from 1.8% to 11.0%). Even more concerning is that it exceeds 7% in the most V contaminated samples. The bioaccessibility of V in ALF solution increases up to 36.7%, which was observed in sample A3, which also contains high total V concentrations. DIPA showed that the highest V bioaccessibility in all samples could be ascribed to the partial digestion of metallic Fe with Cr and V, followed by Ca-Fe-Al-V-oxides with Cr and Ca-Fe-V-oxides with Ti, which were dissolved completely during exposure to ALF solution.

Total Ni concentrations ranged from 44.3 mg kg^{-1} in the reference point (REF-W) to 210 mg kg^{-1} in the most polluted sample in the Ferrobank industrial area (FB2). The bioaccessibility of Ni in GS solution was below the LOD (<0.1 mg kg^{-1}) in half of the samples and increased up to 6.9% in the less polluted samples. The bioaccessibility of Ni in ALF ranges from 6.0% to 19% and is poorly correlated with total Ni levels (Fig. 6). DIPA showed only one phase containing Ni, which is metallic Fe with minor Cr and Ni (0.8 wt% Ni), which dissolved completely in ALF solution.

Co in RD can also be linked to the Witbank smelting industry. Total Co concentrations correlate strongly with total Ni concentrations, while moderate correlations were found for Fe, Cr, and V (Table S3). While the solubility of Co in GS solution is below LOD (<0.2 mg kg^{-1}) for all samples, the bioaccessibility of Co in ALF solution in less polluted samples is comparable to those found by Pelfrêne et al. (2017). However, it is much lower in RD samples from areas polluted by the smelting industry. The bioaccessibility of various Co compounds (salts, driers, pigments, powders, and alloys) in different human surrogate tissue fluids was investigated by Stopford et al. (2003).The results were consistent with the results of our study, where we found that (Mn, Ba)-oxides with Co in RD were completely dissolved in ALF solution.

4.2. Concentrations and inhalation bioaccessibility of elements associated with traffic emissions

The main source of RD pollution with Cu, Zn, Pb, Sb, Sn and Cd in the study area is the traffic emissions (Žibret et al., 2013). The total metal concentrations (Zn ≫ Cu > Pb ≫ Sn > Sb ≫ Cd; Table S3) in the RD samples used in our study are similar to data published in other studies (Amato et al., 2009). The solubility of these elements in GS solution is below the LOD for almost all samples (Table S4). However, the bioaccessibility of these elements in ALF solution is generally much higher compared to the bioaccessibility of elements associated with smelting industry pollution (Table S5, Fig. S2). A strong positive correlation of bioaccessibility was observed for the Cu-Sb ($r_s = 0.72$), Cu-Sn ($r_s = 0.74$), and Sb-Sn ($r_s = 0.85$) pairs. The highest bioaccessibility in ALF solution was observed for Cd, followed by Zn, Pb, Sb, Sn, and Cu.

Cu is one of the main components of car brake pads and is found in concentrations ranging from 11 mg kg^{-1} to 234 000 mg kg^{-1} depending on the manufacturer and pad type (Thorpe and Harrison, 2008). It is also found in tyre treads (from <1 mg kg^{-1} to 490 mg kg^{-1}) and in unleaded gasoline and diesel exhaust. Of all the elements associated with traffic-related pollution, Cu is the only element for which concentrations above the LOD (<0.1 mg kg^{-1}) were detected in the GS extracts of a few samples. The bioaccessibility of Cu in ALF solution is the lowest among the traffic emissions-related metals. However, the bioaccessibility of Cu in sample A1 (Fig. S2), which contains the highest total concentration of Cu, is almost 40%. Copper was found in Fe-Cu-sulphides (chalcopyrite), which showed no visible dissolution after ALF reaction using DIPA, but minute precipitates of Cu-sulphide (covellite) formed on its surface, indicating leaching of Cu from other Cu carriers.

The most important traffic related-source of Zn is tyre and brake pad wear, as the Zn concentration in tyre treads can be as high as 9640 mg kg^{-1}, while brake pads can contain up to 188 000 mg kg^{-1} of Zn (Thorpe and Harrison, 2008). After rain events, when the mobile mass of RD decreases drastically, the recovery of tyre wear particles (organic carbon and zinc) is faster than other RD particles (Amato et al., 2013a,b). Except for the RD sample, which is most contaminated with Zn, the Zn concentrations in the GS extracts are below the LOD (<1 mg kg^{-1}). Zinc was identified as the second most mobile traffic emission-related metal in RD in our study, with observed ALF bioaccessibility ranging from 20% to 66%. A moderate positive correlation ($r_s > 0.50$) was observed between the bioaccessibility of Zn and Pb or Sb. The DIPA analysis showed that only Mn-Al-silicates with Zn and Fe-Al-Zn-silicates contributed to ALF bioaccessibility, as they were partly dissolved (6%–13% reduction in size).

Before alkyl-Pb compounds were banned as anti-knock additives for gasoline, traffic emissions were the main source of urban Pb exposure (Smichowski et al., 2007; Body et al., 1991). The use of leaded gasoline has been significantly prolonged in certain parts of the world. Nowadays, Pb emissions are mainly due to wear and tear of vehicle parts (Loganathan et al., 2013), but resuspended soil along roads, which still contains high Pb levels, can also be an important source of Pb pollution in RD. The total Pb concentrations in the RD samples used in our study are quite low compared to the data from the literature (Pelfrêne et al., 2017; Dean et al., 2017; Potgieter-Vermaak et al., 2012). The measured Pb concentrations in the GS extract were below the LOD (<0.1 mg kg^{-1}), which corresponds to other studies where the measured bioaccessibility of Pb in epithelial lung fluid is very low (Dean et al., 2017; Pelfrêne et al., 2017). A much higher bioaccessibility of Pb was observed in the ALF solution (Fig. S2, Table S5). It ranged from 26% (A12) to a staggering 95% in sample A1, which was collected near the highway. This sample also contains high levels of other elements associated with traffic and also shows the highest ALF bioaccessibility of Cu, Pb, and Sn. According to DIPA, metallic Pb contributed the most to ALF bioaccessibility, as it completely dissolved.

Antimony as Sb_2S_3 is used as a lubricant in brake pads in proportions of up to 7% to reduce vibration and decrease frictional stability (Smichowski et al., 2007; Loganathan et al., 2013; Thorpe and Harrison, 2008). In addition to a number of alloys used in engine bearings, Sb_2O_3 is also used in the vulcanization of rubber as a flame retardant. The recovery of Sb in RD after rain events is slower than for other brake wear tracers such as Sn and Cu (Amato et al., 2013a,b). The reason could be the higher solubility of Sb_2O_3, the oxidation product of Sb_2S_3 in brake

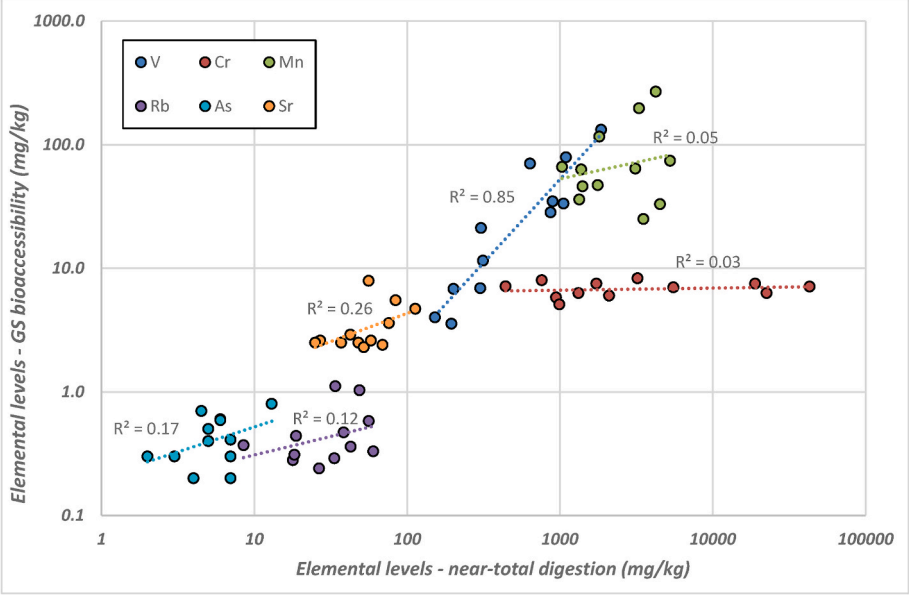

Fig. 5. Scaling of total and bioaccessible fraction in GS solution.

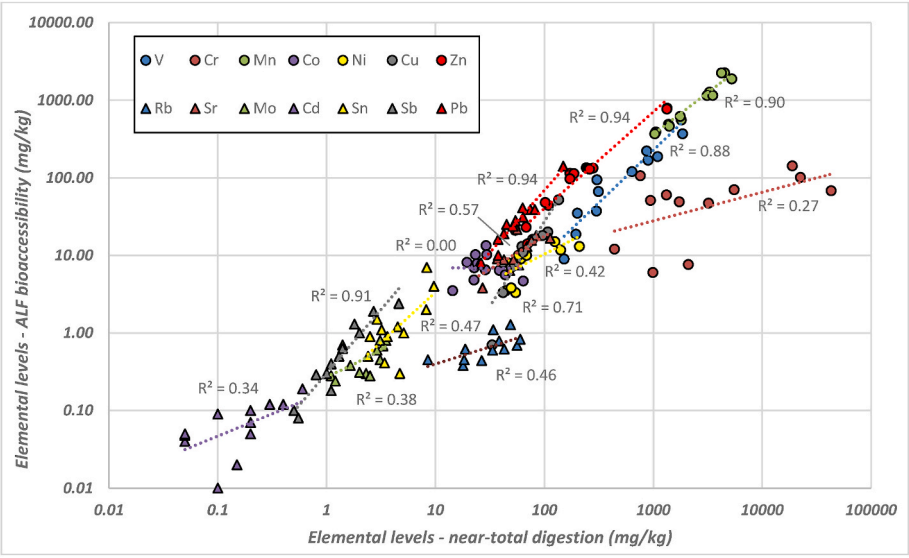

Fig. 6. Scaling of total and bioaccessible fraction in ALF solution.

pad wear, compared to SnO and metallic Cu. The total Sb concentrations in the samples of our study are low compared to published data (Padoan et al., 2017). A high diversity in ALF bioaccessibility was also observed for Sb (Table S5), which is strongly correlated with the ALF bioaccessibility of Cu ($r_s = 0.72$) and Sb ($r_s = 0.85$). No Sb-bearing phases were found using DIPA.

Tin (as SnS) is a component of the underlayer brake pads or is added as a lubricant (Sager, 2020). The recovery of Sn content in RD after rain events is higher than that of Sb (Amato et al., 2013a,b). The mean total Sn concentration in the RD of our study is three times higher than the mean content of Sb (Table S3), and is comparable to other studies (Alves et al., 2020). The concentrations of Sn in GS extracts of RD are below the LOD (<0.05 mg kg^{-1}), while the bioaccessibility in ALF ranges from 6.9% to 79%. Literature data on the inhalation bioaccessibility of Sn in RD are negligible. No Sn-containing phases were found using DIPA.

Cadmium is also a component of brake pads (8–12 mg kg^{-1}) and tyre treads (<0.05–2.6 mg kg^{-1}) (Loganathan et al., 2013). The total concentrations of Cd in our RD samples ranged from 0.05 mg kg^{-1} to 0.6 mg kg^{-1}. The highest bioaccessibility (up to 97%) of Cd was observed in the samples with low total Cd levels but are heavily polluted with other elements associated with the metal smelting industry. The results are consistent with the literature, which generally reports quite low concentrations of Cd in RD (<0.5 mg kg^{-1}) and indicates that Cd has fairly high mobility (Zhang et al., 2015; Jayarathne et al., 2017). No Cd-bearing phases were observed using DIPA.

The scaling of the total amount of PTE and the bioaccessible fraction in the GS (Fig. 5) and ALF solution (Fig. 6) indicates varying degrees of correlation and different slopes of the regression lines. The highest positive correlation between concentrations in GS solution and total concentrations was observed for V. The other elements do not show statistically significant correlations. This can be interpreted as indicating that V levels are highly influenced by the vanadium smelting operations and emissions from this plant show a high degree of bioaccessible fraction in GS solution. For other elements, it might be speculated that there are multiple sources of these metals, each containing various bioaccessible fractions. Considering bioaccessibility in the ALF solution,

the highest correlations between the total and the bioaccessible levels were observed for Zn, Pb, Sb, Mn and V. The corresponding correlation coefficients were 0.94, 0.94, 0.91, 0.90 and 0.88 respectively (Fig. 6). Zn, Pb, and Sb are typical for traffic emissions, while Mn and V are typical for the smelting industry.

This study emphasized the need to consider not only total concentrations of elements in RD, but also their bioaccessible fraction. The bioaccessible fractions of various PTE vary drastically between elements and between samples. Each source of PTE has its own characteristics in terms of bioaccessibility. However, the determination of inhalation bioaccessibility would be more appropriate for the PM10 or PM2.5 fraction of RD, even though the fraction <0.125 mm was utilized in this study. The decision was made for the following reasons: i) to ensure direct comparability with the previous results that used the <0.125 mm fraction, ii) extracting PM10 or PM2.5 particles from a bulk sample with <0.125 mm grain size is practically impossible considering the amount of material we had on our disposal, iii) working with PM10 or PM2.5 particles under the fume hood would be very challenging if not impossible, and iv) working with particle sizes of <0.125 mm is more convenient for applying DIPA. In order to meet the objectives of our study, which was to investigate which phases are affected by simulated lung fluids and connect them to the specific sources, it was found that a grain size <0.125 mm is appropriate. Considering the argument, that grain sizes between 0.010 and 0.125 mm are rarely inhaled, the results of total bioavailability of PTE in RD samples in this study might not represent the actual inhalation bioavailability. An opposing argument could be that larger particles have a much smaller specific surface area for the reaction and, thus, do not contribute significantly to the total bioavailability compared to smaller particles. This could be a topic for further studies, as well as addressing the question regarding bioaccessibility of PTE in RD, as the author believes this is an important source of PTE exposure in urban areas.

5. Conclusion

RD is becoming a widely recognised proxy for the atmospheric PM composition and acts as a sink and source of atmospheric particles, especially in the urban environment. The pathways of PTE into the human body are via dermal contact, ingestion, and, most importantly, inhalation. The findings of nearly every RD study worldwide indicate a high presence of PTE in this medium, but only a few of them address the inhalation bioaccessibility of metals. The RD in this study was collected from highly contaminated areas due to the presence of smelters, mining and traffic. These areas contain some of the highest levels of Cr and V globally. While the measured bioaccessibility of PTE in the GS solution is below the LOD or very low for most samples (up to 11% for V), the mobility of PTE in the ALF solution was much higher (up to 98.8% in the case of Cd). The main findings of this study indicate that the most bioaccessible metals (>40%) were those most probably related to traffic emissions (Zn, Pb, Sb). Intermediate inhalation bioaccessibility (>20% and <40%) was observed for Cd, Mn, Sn, Co and Cu. In contrast, low inhalation bioaccessibility (<20%) was found for elements emitted from the smelting industry (V, Fe, Ni and Cr). Comparison of the individual particles before and after applying the ALF solution with DIPA under SEM/EDS revealed that 40% of the phase species underwent significant physico-chemical property changes. Polymetallic oxides and silicates were found to be the most unstable in ALF digestion. The results suggest that natural phases are more stable, while technogenic phases show a larger proportion of changes after the application of ALF solution. The crystallinity, the type of chemical bonding, and the composition of particulate phases can play a very important role in determining bioaccessibility of metals. This study is important for improving future assessment of the health impacts of inhaling contaminated RD worldwide.

CRediT authorship contribution statement

Marija Zupančič: Writing – review & editing, Writing – original draft, Visualization, Supervision, Resources, Methodology, Investigation, Formal analysis, Data curation, Conceptualization. **Miloš Miler:** Writing – review & editing, Writing – original draft, Visualization, Supervision, Resources, Methodology, Investigation, Formal analysis, Data curation, Conceptualization. **Gorazd Žibret:** Writing – review & editing, Writing – original draft, Visualization, Project administration, Funding acquisition, Formal analysis, Conceptualization.

Declaration of competing interest

The authors declare that they have no known competing financial interests or personal relationships that could have appeared to influence the work reported in this paper.

Data availability

Data will be made available on request.

Acknowledgements

Part of the research was carried out using equipment from the Network of Research Infrastructure Centres of the University of Ljubljana (MRIC UL). The authors would like to thank the Slovenian Research and Innovation Agency (ARIS) for the financial support of MRIC UL and for the financial support from the research programmes P1-0134b Chemistry for Sustainable Development, P1-0025 Mineral resources and research project J1-1713 Dynamics and matter flow of potentially toxic elements (PTEs) in urban environment. Sampling was done within the project EO-MINERS, co-funded by the EU by 7th Framework Programme (grant agreement ID: 244242).

Appendix A. Supplementary data

Supplementary data to this article can be found online at https://doi.org/10.1016/j.envpol.2024.124810.

References

Africa GeoPortal, 2023. 1:1,000,000 scale geology for South Africa. https://www.africageoportal.com/maps/esriza::11000000-geological-map/explore?location=-25.866294%2C29.255636%2C11.77. (Accessed 23 July 2024).

Ali, M.U., Liu, G., Yousaf, B., Abbas, Q., Ullah, H., Munir, M.A.M., et al., 2017. Pollution characteristics and human health risks of potentially (eco)toxic elements (PTEs) in road dust from metropolitan area of Hefei, China. Chemosphere 181, 111–121. https://doi.org/10.1016/j.chemosphere.2017.04.061.

Alves, C.A., Vicente, E.D., Vicente, A.M.P., Rienda, I.C., Tome, M., Querol, X., et al., 2020. Loadings, chemical patterns and risks of inhalable road dust particles in an Atlantic city in the north of Portugal (Article). Sci. Total Environ. 737, 12. https://doi.org/10.1016/j.scitotenv.2020.139596.

Amato, F., Pandolfi, M., Viana, M., Querol, X., Alastuey, A., Moreno, T., 2009. Spatial and chemical patterns of PM10 in road dust deposited in urban environment. Atmos. Environ. 43 (9), 1650–1659. https://doi.org/10.1016/j.atmosenv.2008.12.009.

Amato, F., Pandolfi, M., Alastuey, A., Lozano, A., Contreras González, J., Querol, X., 2013a. Impact of traffic intensity and pavement aggregate size on road dust particles loading. Atmos. Environ. 77, 711–717. https://doi.org/10.1016/j.atmosenv.2013.05.020.

Amato, F., Schaap, M., Denier van der Gon, H.A.C., Pandolfi, M., Alastuey, A., Keuken, M., et al., 2013b. Short-term variability of mineral dust, metals and carbon emission from road dust resuspension. Atmos. Environ. 74, 134–140. https://doi.org/10.1016/j.atmosenv.2013.03.037.

Anthony, J.W., Bideaux, R.A., Bladh, K.W., Nichols, M.C., 2009. In: 'Handbook of Mineralogy' J. W. Anthony, R. A. Bideaux, K. W. Bladh, & M. C. Nichols. Chantilly, VA 20151-1110. Mineralogical Society of America, USA. Available at: http://www.handbookofmineralogy.org/.

Bardelli, F., Cattaruzza, E., Gonella, F., Rampazzo, G., Valotto, G., 2011. Characterization of road dust collected in Traforo del San Bernardo highway tunnel: Fe and Mn speciation. Atmos. Environ. 45 (35), 6459–6468. https://doi.org/10.1016/j.atmosenv.2011.07.035.

Barrett, J.E.S., Taylor, K.G., Hudson-Edwards, K.A., Charnock, J.M., 2010. Solid-phase speciation of Pb in urban road dust sediment: a xanes and EXAFS study. Environ. Sci. Technol. 44 (8), 2940–2946. https://doi.org/10.1021/es903737k.

Barthelmy, D., 2012. The mineralogy database. Available at: https://webmineral.com/.

Body, P.E., Inglis, G., Dolan, P.R., Mulcahy, D.E., 1991. Environmental lead: a review. Crit. Rev. Environ. Control 20 (5–6), 299–310. https://doi.org/10.1080/10643389109388403.

Boim, A.G.F., Patinha, C., Wragg, J., Cave, M., Alleoni, L.R.F., 2021. Respiratory bioaccessibility and solid phase partitioning of potentially harmful elements in urban environmental matrices. Sci. Total Environ. 765, 142791 https://doi.org/10.1016/j.scitotenv.2020.142791.

Caboche, J., Perdrix, E., Malet, B., Laurent, A.Y., 2011. Development of an in vitro method to estimate lung bioaccessibility of metals from atmospheric particles. J. Environ. Monit. 13 (3), 621–630. https://doi.org/10.1039/C0EM00439A.

Cánovas, C.R., Quispe, D., Macías, F., Callejón-Leblic, B., Arias-Borrego, A., García-Barrera, T., et al., 2023. Potential release and bioaccessibility of metal/loids from mine wastes deposited in historical abandoned sulfide mines. Environ. Pollut. 316, 120629 https://doi.org/10.1016/j.envpol.2022.120629.

Chen, L., Fang, L., Yang, X., Luo, X., Qiu, T., Zeng, Y., et al., 2024. Sources and human health risks associated with potentially toxic elements (PTEs) in urban dust: a global perspective. Environ. Int. 187, 108708 https://doi.org/10.1016/j.envint.2024.108708.

Cipullo, S., Prpich, G., Campo, P., Coulon, F., 2018. Assessing bioavailability of complex chemical mixtures in contaminated soils: progress made and research needs. Sci. Total Environ. 615, 708–723. https://doi.org/10.1016/j.scitotenv.2017.09.321.

Colombo, C., Monhemius, A.J., Plant, J.A., 2008. Platinum, palladium and rhodium release from vehicle exhaust catalysts and road dust exposed to simulated lung fluids. Ecotoxicol. Environ. Saf. 71 (3), 722–730. https://doi.org/10.1016/j.ecoenv.2007.11.011.

Corona-Sánchez, J.E., González-Chávez, M.d.C.A., Carrillo-González, R., García-Cué, J. L., Fernández-Reynoso, D.S., Noerpel, M., et al., 2021. Bioaccessibility of potentially toxic elements in mine residue particles (10.1039/D0EM00447B). Environmental Science: Process. Impacts 23 (2), 367–380. https://doi.org/10.1039/D0EM00447B.

Corradi, M., Mutti, A., 2011. Metal ions affecting the pulmonary and cardiovascular systems. In: Sigel, A., Sigel, H., Sigel Roland, K.O. (Eds.), Metal Ions in Toxicology: Effects, Interactions, Interdependencies. Royal Society of Chemistry, pp. 81–105. https://doi.org/10.1515/9783110436624-009.

Dean, J.R., Elom, N.I., Entwistle, J.A., 2017. Use of simulated epithelial lung fluid in assessing the human health risk of Pb in urban street dust. Sci. Total Environ. 579, 387–395. https://doi.org/10.1016/j.scitotenv.2016.11.085.

Dehghani, S., Moore, F., Keshavarzi, B., Hale, B.A., 2017. Health risk implications of potentially toxic metals in street dust and surface soil of Tehran, Iran. Ecotoxicol. Environ. Saf. 136, 92–103. https://doi.org/10.1016/j.ecoenv.2016.10.037.

Diao, J., Xie, B., Wang, Y., Ji, C.Q., 2009. Mineralogical characterisation of vanadium slag under different treatment conditions. Ironmak. Steelmak. 36 (6), 476–480. https://doi.org/10.1179/174328109X410622.

Dietrich, M., O'Shea, M.J., Gieré, R., Krekeler, M.P.S., 2022. Road sediment, an underutilized material in environmental science research: a review of perspectives on United States studies with international context. J. Hazard Mater. 432, 128604 https://doi.org/10.1016/j.jhazmat.2022.128604.

Drysdale, M., Ljung Bjorklund, K., Jamieson, H.E., Weinstein, P., Cook, A., Watkins, R.T., 2012. Evaluating the respiratory bioaccessibility of nickel in soil through the use of a simulated lung fluid. Environ. Geochem. Health 34 (2), 279–288. https://doi.org/10.1007/s10653-011-9435-x.

Duong, T.T.T., Lee, B.-K., 2009. Partitioning and mobility behavior of metals in road dusts from national-scale industrial areas in Korea. Atmos. Environ. 43 (22), 3502–3509. https://doi.org/10.1016/j.atmosenv.2009.04.036.

Egodawatta, P., Goonetilleke, A., 2008. Understanding road surface pollutant wash-off and underlying physical processes using simulated rainfall. Water Sci. Technol. 57 (8), 1241–1246. https://doi.org/10.2166/wst.2008.260.

Entwistle, J.A., Hursthouse, A.S., Reis, P.A.M., Stewart, A.G., 2019. Metalliferous mine dust: human health impacts and the potential determinants of disease in mining communities (article). Current Pollution Reports 5 (3), 67–83. https://doi.org/10.1007/s40726-019-00108-5.

Expósito, A., Markiv, B., Ruiz-Azcona, L., Santibáñez, M., Fernández-Olmo, I., 2021. Understanding how methodological aspects affect the release of trace metal(loid)s from urban dust in inhalation bioaccessibility tests. Chemosphere 267, 129181. https://doi.org/10.1016/j.chemosphere.2020.129181.

Gaberšek, M., Gosar, M., 2024. Oral bioaccessibility of potentially toxic elements in various environmental media. Environ. Geochem. Health 46, 21. https://doi.org/10.1007/s10653-024-02073-5.

Gao, F., Olayiwola, A.U., Liu, B., Wang, S., Du, H., Li, J., et al., 2021. Review of vanadium production Part I: primary resources. Miner. Process. Extr. Metall. Rev. 43 (4), 466–488. https://doi.org/10.1080/08827508.2021.1883013.

Gunawardana, C., Goonetilleke, A., Egodawatta, P., Dawes, L., Kokot, S., 2012. Source characterisation of road dust based on chemical and mineralogical composition. Chemosphere 87 (2), 163–170. https://doi.org/10.1016/j.chemosphere.2011.12.012.

Goldstein, J., Newbury, D., Joy, D., Lyman, C., Echlin, P., Lifshin, E., et al., 2003. Scanning electron microscopy and X-ray microanalysis, 3rd edition. Kluwer Academic/Plenum Publishers, New York.

Gunawardana, C., Egodawatta, P., Goonetilleke, A., 2015. Adsorption and mobility of metals in build-up on road surfaces. Chemosphere 119, 1391–1398. https://doi.org/10.1016/j.chemosphere.2014.02.048.

Guney, M., Chapuis, R.P., Zagury, G.J., 2016. Lung bioaccessibility of contaminants in particulate matter of geological origin. Environ. Sci. Pollut. Control Ser. 23 (24), 24422–24434. https://doi.org/10.1007/s11356-016-6623-3.

Guney, M., Bourges, C.M.J., Chapuis, R.P., Zagury, G.J., 2017. Lung bioaccessibility of As, Cu, Fe, Mn, Ni, Pb, and Zn in fine fraction (<20μm) from contaminated soils and mine tailings. Sci. Total Environ. 579, 378–386. https://doi.org/10.1016/j.scitotenv.2016.11.086.

Hancox, P.J., 2016. The coalfields of South-central Africa: a current perspective (article). Episodes 39 (2), 407–428. https://doi.org/10.18814/epiiugs/2016/v39i2/95785.

Hedberg, Y., Gustafsson, J., Karlsson, H.L., Möller, L., Odnevall Wallinder, I., 2010. Bioaccessibility, bioavailability and toxicity of commercially relevant iron- and chromium-based particles: in vitro studies with an inhalation perspective. Part. Fibre Toxicol. 7, 23. https://doi.org/10.1186/1743-8977-7-23, 23.

Horckmans, L., Möckel, R., Nielsen, P., Kukurugya, F., Vanhoof, C., Morillon, A., et al., 2019. Multi-analytical characterization of slags to determine the chromium concentration for a possible Re-extraction. Minerals 9 (10), 646. https://doi.org/10.3390/min9100646.

Hunt, A., Johnson, D.L., 2011. Differential individual particle analysis (DIPA): applications in particulate matter characterization. J. Environ. Qual. 40 (3), 742–750. https://doi.org/10.2134/jeq2010.0315.

INCA, 2006. INCA Energy Operator Manual. Oxford Instruments analytical Ltd. High Wycombe.

Jayarathne, A., Egodawatta, P., Ayoko, G.A., Goonetilleke, A., 2017. Geochemical phase and particle size relationships of metals in urban road dust. Environ. Pollut. 230, 218–226. https://doi.org/10.1016/j.envpol.2017.06.059.

Jayarathne, A., Egodawatta, P., Ayoko, G.A., Goonetilleke, A., 2018a. Assessment of ecological and human health risks of metals in urban road dust based on geochemical fractionation and potential bioavailability. Sci. Total Environ. 635, 1609–1619. https://doi.org/10.1016/j.scitotenv.2018.04.098.

Jayarathne, A., Egodawatta, P., Ayoko, G.A., Goonetilleke, A., 2018b. Role of residence time on the transformation of Zn, Cu, Pb and Cd attached to road dust in different land uses. Ecotoxicol. Environ. Saf. 153, 195–203. https://doi.org/10.1016/j.ecoenv.2018.02.007.

Jayarathne, A., Egodawatta, P., Ayoko, G.A., Goonetilleke, A., 2019a. Transformation processes of metals associated with urban road dust: a critical review. Crit. Rev. Environ. Sci. Technol. 49 (18), 1675–1699. https://doi.org/10.1080/10643389.2019.1579630.

Jayarathne, A., Wijesiri, B., Egodawatta, P., Ayoko, G.A., Goonetilleke, A., 2019b. Role of adsorption behavior on metal build-up in urban road dust. J. Environ. Sci. 83, 85–95. https://doi.org/10.1016/j.jes.2019.03.023.

JMA Consulting, 2014. Samancor chrome ferrometals environmental impact assessment & environmental management programme, final report. JMA Consulting (Pty) Ltd. Delmas, SA, pp. 1–206.

Kastury, F., Smith, E., Juhasz, A.L., 2017. A critical review of approaches and limitations of inhalation bioavailability and bioaccessibility of metal(loid)s from ambient particulate matter or dust. Sci. Total Environ. 574, 1054–1074. https://doi.org/10.1016/j.scitotenv.2016.09.056.

Kastury, F., Karna, R.R., Scheckel, K.G., Juhasz, A.L., 2020a. Correlation between lead speciation and inhalation bioaccessibility using two different simulated lung fluids. Environ. Pollut. 263, 114609 https://doi.org/10.1016/j.envpol.2020.114609.

Kastury, F., Ritch, S., Rasmussen, P.E., Juhasz, A.L., 2020b. Influence of household smoking habits on inhalation bioaccessibility of trace elements and light rare earth elements in Canadian house dust. Environ. Pollut. 262, 114132 https://doi.org/10.1016/j.envpol.2020.114132.

Liu, E., Yan, T., Birch, G., Zhu, Y., 2014. Pollution and health risk of potentially toxic metals in urban road dust in Nanjing, a mega-city of China. Sci. Total Environ. 476–477, 522–531. https://doi.org/10.1016/j.scitotenv.2014.01.055.

Loganathan, P., Vigneswaran, S., Kandasamy, J., 2013. Road-deposited sediment pollutants: a critical review of their characteristics, source apportionment, and management. Crit. Rev. Environ. Sci. Technol. 43 (13), 1315–1348. https://doi.org/10.1080/10643389.2011.644222.

Mahbub, P., Ayoko, G.A., Goonetilleke, A., Egodawatta, P., Kokot, S., 2010. Impacts of traffic and rainfall characteristics on heavy metals build-up and wash-off from urban roads. Environ. Sci. Technol. 44 (23), 8904–8910. https://doi.org/10.1021/es1012565.

Miler, M., 2021. Airborne particles in city bus: concentrations, sources and simulated pulmonary solubility. Environ. Geochem. Health 43 (7), 2757–2780. https://doi.org/10.1007/s10653-020-00770-5.

Mokwena, M.L., 2012. The Occurrence of Chromium and Other Trace Elements in Selected South African Coals. Master's Dissertation. University of Johannesburg, Johannesburg. https://hdl.handle.net/10210/401413.

Monneron-Gyurits, M., Soubrand, M., Joussein, E., Courtin, A., Paineau, E., Reguer, S., et al., 2024. Relation between solid phase speciation and oral/lung bioaccessibility of metal(loid)s polluted soils in inhabited area: contribution of synchrotron-based experiment. Sci. Total Environ. 930, 172765 https://doi.org/10.1016/j.scitotenv.2024.172765.

Nkohla, M.A., 2006. Characteristics of Ferrochrome Smelter Slag and its Implications in Metal Accounting. Cape Peninsula University of Technology. Thesis. http://hdl.handle.net/20.500.11838/877.

Novo-Quiza, N., Sanromán-Hermida, S., Sánchez-Piñero, J., Moreda-Piñeiro, J., Muniategui-Lorenzo, S., López-Mahía, P., 2023. In-vitro inhalation bioavailability estimation of Metal(oid)s in atmospheric particulate matter (PM2.5) using simulated alveolar lysosomal fluid: a dialyzability approach. Environ. Pollut. 317, 120761 https://doi.org/10.1016/j.envpol.2022.120761.

Padoan, E., Romè, C., Ajmone-Marsan, F., 2017. Bioaccessibility and size distribution of metals in road dust and roadside soils along a peri-urban transect. Sci. Total Environ. 601–602, 89–98. https://doi.org/10.1016/j.scitotenv.2017.05.180.

Pelfrêne, A., Douay, F., 2018. Assessment of oral and lung bioaccessibility of Cd and Pb from smelter-impacted dust. Environ. Sci. Pollut. Control Ser. 25 (4), 3718–3730. https://doi.org/10.1007/s11356-017-0760-1.

Pelfrêne, A., Cave, M.R., Wragg, J., Douay, F., 2017. In vitro investigations of human bioaccessibility from reference materials using simulated lung fluids. Int. J. Environ. Res. Publ. Health 14 (2), 112. https://doi.org/10.3390/ijerph14020112.

Perimal, M., 2013. South African Iron & Steel Institute. https://saisi.co.za/hiveld.php. (Accessed 23 July 2024).

Potgieter-Vermaak, S., Rotondo, G., Novakovic, V., Rollins, S., Van Grieken, R., 2012. Component-specific toxic concerns of the inhalable fraction of urban road dust. Environ. Geochem. Health 34 (6), 689–696. https://doi.org/10.1007/s10653-012-9488-5.

Ringdalen, E., Rocha, M., Neto, J.R., Malvik, T., 2013. Properties of chromite ores from Ferbasa and their effect on Cr-losses to slag during HCFeCr production at Ferbasa. In: Proceedings of 13th International Ferroalloys Congress INFACON on Efficient Technologies in Ferroalloy Industry. Public Association INFACON XIII. Almaty, pp. 115–125. https://pyrometallurgy.co.za/InfaconXIII/0115-Ringdalen.pdf.

Sager, M., 2020. Urban soils and road dust—civilization effects and metal pollution—a review. Environments 7 (11). https://doi.org/10.3390/environments7110098.

Samancor Chrome, 2018. Samancor Products. https://samancorcr.com/products/. (Accessed 23 July 2024).

Shi, G., Chen, Z., Bi, C., Wang, L., Teng, J., Li, Y., et al., 2011. A comparative study of health risk of potentially toxic metals in urban and suburban road dust in the most populated city of China. Atmos. Environ. 45 (3), 764–771. https://doi.org/10.1016/j.atmosenv.2010.08.039.

Smichowski, P., Gómez, D., Frazzoli, C., Caroli, S., 2007. Traffic-related elements in airborne particulate matter. Appl. Spectrosc. Rev. 43 (1), 23–49. https://doi.org/10.1080/05704920701645886.

Steinberg, W.S., Geyser, W., Nell, J., 2011. The history and development of the pyrometallurgical processes at Evraz Highveld Steel & Vanadium. J. S. Afr. Inst. Min. Metall 111 (10), 705–710. https://www.scielo.org.za/scielo.php?script=sci_arttext&pid=S2225-62532011001000009.

Stopford, W., Turner, J., Cappellini, D., Brock, T., 2003. Bioaccessibility testing of cobalt compounds (10.1039/B302257A). J. Environ. Monit. 5 (4), 675–680. https://doi.org/10.1039/B302257A.

Świetlik, R., Trojanowska, M., Strzelecka, M., Bocho-Janiszewska, A., 2015. Fractionation and mobility of Cu, Fe, Mn, Pb and Zn in the road dust retained on noise barriers along expressway – a potential tool for determining the effects of driving conditions on speciation of emitted particulate metals. Environ. Pollut. 196, 404–413. https://doi.org/10.1016/j.envpol.2014.10.018.

Teran, K., Žibret, G., Fanetti, M., 2020. Impact of urbanization and steel mill emissions on elemental composition of street dust and corresponding particle characterization. J. Hazard Mater. 384, 120963 https://doi.org/10.1016/j.jhazmat.2019.120963.

Thorpe, A., Harrison, R.M., 2008. Sources and properties of non-exhaust particulate matter from road traffic: a review. Sci. Total Environ. 400 (1), 270–282. https://doi.org/10.1016/j.scitotenv.2008.06.007.

Trojanowska, M., Swietlik, R., 2020. Investigations of the chemical distribution of heavy metals in street dust and its impact on risk assessment for human health, case study of Radom (Poland). Human and Ecological Risk Assessment 26 (7), 1907–1926. https://doi.org/10.1080/10807039.2019.1619070.

Weggeberg, H., Benden, T.F., Lierhagen, S., Steinnes, E., Flaten, T.P., 2019. Characterization and bioaccessibility assessment of elements in urban aerosols by extraction with simulated lung fluids. Environmental Chemistry and Ecotoxicology 1, 49–60. https://doi.org/10.1016/j.enceco.2019.10.001.

Wiseman, C.L.S., Niu, J., Levesque, C., Chénier, M., Rasmussen, P.E., 2018. An assessment of the inhalation bioaccessibility of platinum group elements in road dust using a simulated lung fluid. Environ. Pollut. 241, 1009–1017. https://doi.org/10.1016/j.envpol.2018.06.043.

Witt, E.C., Shi, H., Wronkiewicz, D.J., Pavlowsky, R.T., 2014. Phase partitioning and bioaccessibility of Pb in suspended dust from unsurfaced roads in Missouri—a potential tool for determining mitigation response. Atmos. Environ. 88, 90–98. https://doi.org/10.1016/j.atmosenv.2014.02.002.

Yang, H., Liu, Y., Wan, X., Zhang, T., Lin, S., Wang, K., et al., 2023. Microstructure and mineral phase evolution of vanadium slag by modulating the CaO/V2O5 ratio. Minerals 13, 628. https://doi.org/10.3390/min13050628.

Zhang, M., Wang, H., 2009. Concentrations and chemical forms of potentially toxic metals in road-deposited sediments from different zones of Hangzhou, China. J. Environ. Sci. 21 (5), 625–631. https://doi.org/10.1016/S1001-0742(08)62317-7.

Zhang, J., Hua, P., Krebs, P., 2015. The build-up dynamic and chemical fractionation of Cu, Zn and Cd in road-deposited sediment. Sci. Total Environ. 532, 723–732. https://doi.org/10.1016/j.scitotenv.2015.06.074.

Žibret, G., 2019. Influences of coal mines, metallurgical plants, urbanization and lithology on the elemental composition of street dust. Environ. Geochem. Health 41 (3), 1489–1505. https://doi.org/10.1007/s10653-018-0228-3.

Žibret, G., Rokavec, D., 2010. Household dust and street sediment as an indicator of recent heavy metals in atmospheric emissions: a case study on a previously heavily contaminated area. Environ. Earth Sci. 61 (3), 443–453. https://doi.org/10.1007/s12665-009-0356-2.

Žibret, G., Van Tonder, D., Žibret, L., 2013. Metal content in street dust as a reflection of atmospheric dust emissions from coal power plants, metal smelters, and traffic. Environ. Sci. Pollut. Control Ser. 20 (7), 4455–4468. https://doi.org/10.1007/s11356-012-1398-7.

Zupančič, M., Šušteršič, M., Bavec, Š., Gosar, M., 2021. Oral and inhalation bioaccessibility of potentially toxic elements in household dust from former Hg mining district, Idrija, Slovenia. Environ. Geochem. Health 43 (9), 3505–3531. https://doi.org/10.1007/s10653-021-00835-z.